Available online at www.sciencedirect.com
ScienceDirect
Trans. Nonferrous Met. Soc. China 27(2017) 1947−1955
Transactions of Nonferrous Metals Society of China
www.tnmsc.cn

Age-hardening behavior and microstructure of Cu−15Ni−8Sn−0.3Nb alloy prepared by powder metallurgy and hot extrusion

Yi OUYANG[1], Xue-ping GAN[1], Shi-zhong ZHANG[1], Zhou LI[2], Ke-chao ZHOU[1], Ye-xin JIANG[2,3], Xian-wei ZHANG[2,3]

1. State Key Laboratory of Powder Metallurgy, Central South University, Changsha 410083, China;
2. School of Materials Science and Engineering, Central South University, Changsha 410083, China;
3. CNMC Albetter Albronze Co., Ltd., Liaocheng 252600, China

Received 2 January 2017; accepted 5 May 2017

Abstract: Cu−15Ni−8Sn−0.3Nb alloy rods were prepared by means of powder metallurgy followed by hot extrusion. Element maps obtained by electron probe micro analyzer (EPMA) showed that Nb-rich phases were formed and distributed within grains and at grain boundaries of the Cu−15Ni−8Sn−0.3Nb alloy. Transmission electron microscope (TEM) results indicated that there was no obvious orientation relationship between these phases and the matrix. Spinodal decomposition and ordering transformation appeared at early stages of aging at 400 °C and caused significant strengthening. Cu−15Ni−8Sn−0.3Nb alloy exhibited both higher strength (ultimate tensile strength >1030 MPa) and higher tensile ductility (elongation>9.1%) than Cu−15Ni−8Sn alloy after aging treatment. The improvement was caused by Nb-rich phases at grain boundaries which led o the refinement of grain size and postponed the growth of discontinuous precipitates during aging.

Key words: Cu−15Ni−8Sn−0.3Nb alloy; powder metallurgy method; hot extrusion; aging treatment; spinodal decomposition; microstructure; mechanical properties

1 Introduction

Commercial Cu−Ni−Sn alloys have been widely used as springs and connectors in electronic industry and as bearing materials in aerospace, oceaneering and mining industries for their excellent combination of high strength, exceptional bearing properties, stress-relaxation resistance and corrosion-resistance properties [1−3]. Early studies revealed that the age hardening of Cu−Ni−Sn alloys was derived from spinodal decomposition (SD) which occurred at the early stage of aging. During aging treatment, the interplay between internal stress field and dislocations led to substantial strengthening of Cu−Ni−Sn alloys [4−7]. After spinodal decomposition, coherent ordered micro-precipitates with γ'-DO_{22} structure (Al_3Ti type) appeared within minutes [8]. Because of the modulated structure and ordered precipitates, Cu−Ni−Sn alloys with high strength could be obtained after aging treatment for short time [9,10]. However, a sharp drop in ductility usually occurred [11,12]. The modulated structure was subsequently replaced by discontinuous precipitates (DP), which originated from grain boundaries. Discontinuous precipitates consisted of Sn-lean α-phase and lamellar Sn-rich equilibrium γ-phase, $(Cu_xNi_{1-x})_3Sn$ with a DO_3 structure [13]. The existence of discontinuous precipitates usually led to a decrease in strength.

In the past decades, researchers have concentrated on either improving the mechanical properties of Cu−Ni−Sn alloys [14,15] or investigating transformation kinetics and the interplay among different phase-transition products [16,17]. However, the major challenge remains in resolving the contradiction between the strength and ductility of Cu−Ni−Sn alloys after aging treatment. What's more, Cu−Ni−Sn alloys with high Sn content have wide ranges of solidification, which would lead to detrimental solute segregation easily during conventional melting and casting process [18]. In the Ti−Ni alloy system, the introduction of a Nb-rich soft

Foundation item: Project (2016YFB0301400) supported by the National Key Research and Development Program of China; Project (9140A12040515QT48167) supported by the Pre-research Fund of the General Armaments Department of China; Project (CSU20151024) supported by the Innovation-driven Plan of Central South University, China
Corresponding author: Xue-ping GAN; Tel: +86-731-88836303; E-mail: ganxueping@csu.edu.cn
DOI: 10.1016/S1003-6326(17)60219-X

phase was an effective way to improve the mechanical properties of alloys [19,20]. Nb is ductile as a pure metal, which has a very limited solubility in Cu matrix. The addition of Nb might lead to the formation of soft phases within the grains or along the grain boundaries of Cu−Ni−Sn alloys. Therefore, the ductility of the high-strength Cu−15Ni−8Sn alloy might be improved by the addition of Nb. In addition, the solute segregation of alloys could be inhibited by the powder metallurgy method [21]. Therefore, the element Nb was added to the Cu−15Ni−8Sn alloy by means of powder metallurgy to achieve optimized mechanical property in this study.

2 Experimental

2.1 Materials and methods

Cu−15Ni−8Sn−*x*Nb alloy powders (<100 μm, oxygen content: 290×10^{-6}) were provided by Hunan Henji Technology Co., Ltd., China. The chemical composition of the powders is given in Table 1. Firstly, the alloy powders were sealed in rubble molds by isostatic cool pressing at 200 MPa for 20 min. Then, the pressed ingots were vacuum-sintered at 850 °C and 1×10^{-3} Pa for 4 h. As-sintered ingots were machined to cylindrical-shaped samples with a diameter of 123 mm and a length of 190 mm for hot extrusion. Before hot extrusion, the sintered ingots were solution-treated at 830 °C for 6 h. Hot backward extrusion with water-sealing was performed at 830 °C under an extrusion speed of 30 mm/s and an extrusion ratio of 9.5. As-extruded rods were subjected to solution treatment at 850 °C for 1 h and then quenched in water. A hydrogen tube furnace was used for aging treatment at 400 °C for 15 min to 6 h. After aging treatment, the specimens were quenched in water.

Table 1 Chemical composition of Cu−15Ni−8Sn−*x*Nb alloys (mass fraction, %)

Alloy	Ni	Sn	Nb	Cu
Cu−15Ni−8Sn−0.3Nb	15.21	7.79	0.32	Bal.
Cu−15Ni−8Sn	14.30	7.82	−	Bal.

2.2 Microstructure characterization

Optical microscope (OM) images of the specimens after solution and aging treatment were recorded by using a Leica DM4500P metallurgical microscope. The second-phase volume fraction of the aged specimens was approximated as the area fraction of the dark phases in the optical images, which was calculated by Photoshop. At least 300 grains were measured to determine the average grain size of the aged specimens. Transmission electron microscope (TEM) characterizations were conducted by using a Cs-corrected scanning transmission electron microscope (STEM, FEI Titan G2 60−300) operated at 200 kV. TEM specimens were jet-polished in a solution of 30% nitric acid and 70% methanol held at approximately −30 °C [17]. STEM and electron probe micro analysis (EPMA, JXA−8530F) were used to collect element maps.

2.3 Mechanical properties

Round-bar tensile specimens with gauge dimensions of 5 mm in diameter and 25 mm in length were prepared from the central portion of the aged rods. The axial direction of the specimens was parallel to the extrusion direction. According to the ASTM standard E8M for rod specimens, uniaxial tensile tests were performed by using an Instron 8802 tester at a fixed strain rate of 2 mm/min. At least 5 repeated measurements were conducted for each specimen. Prior to tensile tests, specimens were ground using 600- and 2000-grit paper to remove possible oxides on the surface of the specimens.

3 Results and discussion

3.1 OM images

OM images of Cu−15Ni−8Sn−*x*Nb alloys after solution and aging treatment are shown in Fig. 1. Nearly pure supersaturated *α*-phases were obtained for both Cu−15Ni−8Sn−0.3Nb and Cu−15Ni−8Sn alloys after solution treatment, as shown in Figs. 1(a) and (b), respectively. After aging at 400 °C for 0.5 h, a few dark phases appeared at the grain boundaries of both alloys, as marked in Figs. 1(c) and (d). The dark phases were discontinuous precipitates [14,22]. The volume fractions of discontinuous precipitates (DP) were marked at the top right of each image. Some dark spots were observed inside of the grains, as shown in Figs. 1(b) and (d). The dark spots might be intragranular *γ*-precipitates. Figure 1(e) showed that the volume fraction of discontinuous precipitates in the Cu−15Ni−8Sn−0.3Nb alloy remained low after aging for 1 h. However, discontinuous precipitates in the Cu−15Ni−8Sn alloy grew rapidly at the beginning of aging, as shown in Figs. 1(d) and (f). Therefore, the addition of Nb postponed the growth of discontinuous precipitates to a certain degree. Large amounts of matrix were consumed by discontinuous precipitates in both alloys after long-time aging, as shown in Figs. 1(g) and (h).

The mean grain size of each specimen is also shown in Fig. 1. The grain size of the Cu−15Ni−8Sn−0.3Nb alloy was about 11 μm after aging for 1 h and grew slightly to 12.45 μm after aging for 3 h. However, the grains of the Cu−15Ni−8Sn alloy grew from 11.96 to 21.40 μm after aging for 1 h and reached up to 27.01 μm after aging for 3 h. It is obvious that the grain coarsening was inhibited by the addition of Nb element into Cu−15Ni−8Sn alloy.

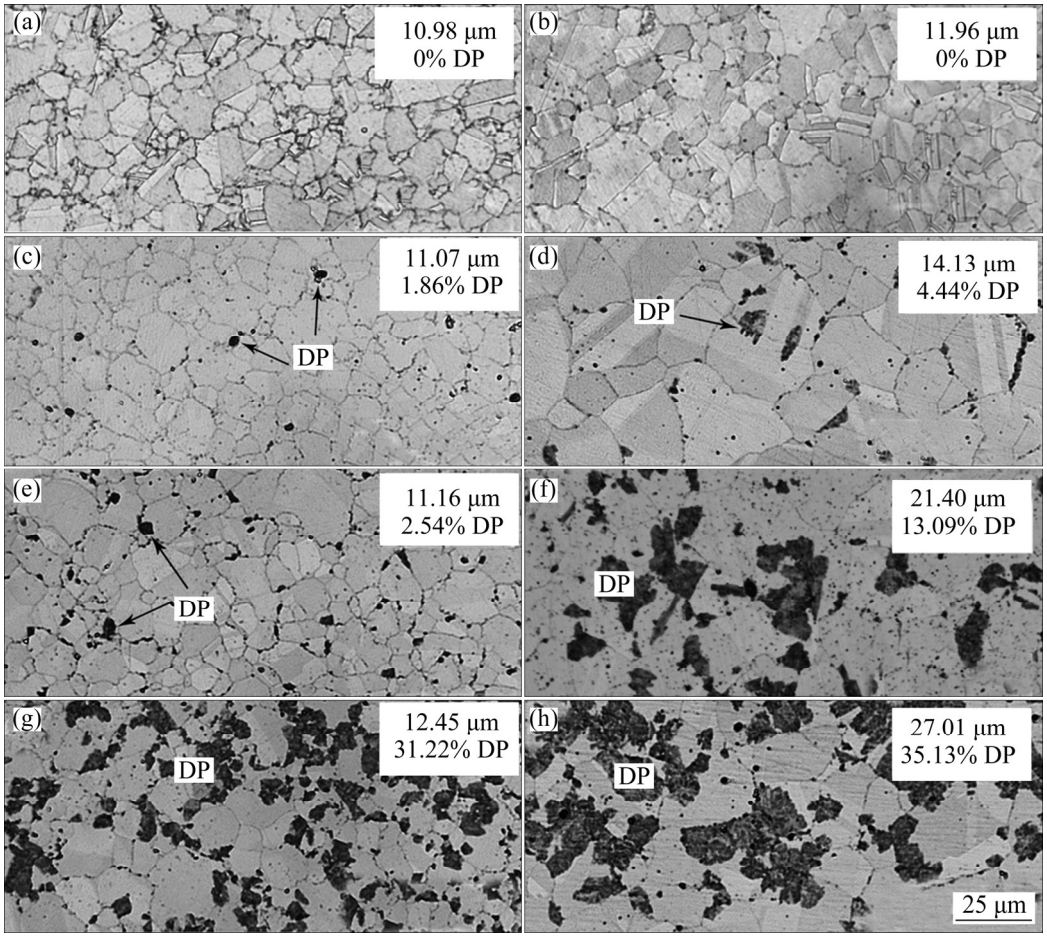

Fig. 1 OM images of Cu−15Ni−8Sn−0.3Nb (a, c, e, g) and Cu−15Ni−8Sn (b, d, f, h) alloys: Solution-treated at 850 °C for 1 h (a, b) and aged at 400 °C for 0.5 h (c, d), 1 h (e, f) and 3 h (g, h)

3.2 EPMA maps

Element maps of the Cu−15Ni−8Sn−0.3Nb alloy were obtained by EPMA tests. Figure 2 shows back-scattered electron (BSE) images and corresponding Nb element maps of the Cu−15Ni−8Sn−0.3Nb alloy. Figure 2(a) presents the BSE image of Cu−15Ni−8Sn−0.3Nb specimen after solution treatment, which indicates the existence of precipitates both inside the grains and at the grain boundaries. The corresponding Nb element map is shown in Fig. 2(c). It can be seen from Fig. 2(c) that Nb element was distributed mainly at the grain boundaries (such as in Position *a*) and a small amount of Nb could be detected within the grains (such as in Position *b*), which could explain the grain-refinement of the Cu−15Ni−8Sn−0.3Nb alloys, as shown in Fig. 1. The *α*-matrix was consumed by discontinuous precipitates after aging at 400 °C for 3 h, as shown in Fig. 2(b). The Nb-rich phases remained at original positions even after the engulfment of discontinuous precipitates, as shown in Fig. 2(d). The Nb-rich phase at Position *c* in Figs. 2(b) and (d) seemed to block the growth of discontinuous precipitates at the position because the matrix beside it was not consumed by discontinuous precipitates. The Nb-rich phase at grain boundaries was a barrier to the grain growth of the Cu−15Ni−8Sn−0.3Nb alloy.

3.3 TEM images

Figure 3 shows the TEM images and the corresponding selected area diffraction pattern (SADP) of the Cu−15Ni−8Sn−0.3Nb alloy specimen aged at 400 °C for 0.25 h. The modulated morphology of the matrix due to spinodal decomposition is shown in Fig. 3(a). The SADP along [001] direction is given in Fig. 3(b). This shows clear superlattice reflections resulted from ordering. It is obvious that the {001}- and {011}-type superlattice reflections in Fig. 3(b) are larger than the {0 1/2 1}-type superlattice reflections. It is well known that the {001}- and {011}-type reflections belong to both DO_{22} and $L1_2$ ordering and the {0 1/2 1}-type reflections only belong to DO_{22} ordering [17]. Therefore, the difference of intensity in the two types of superlattice reflections indicates that the DO_{22} reflections are overlapped by $L1_2$ reflections ({001}- and {011}-types), which means that both DO_{22} and $L1_2$ ordering phases are obtained in this specimen.

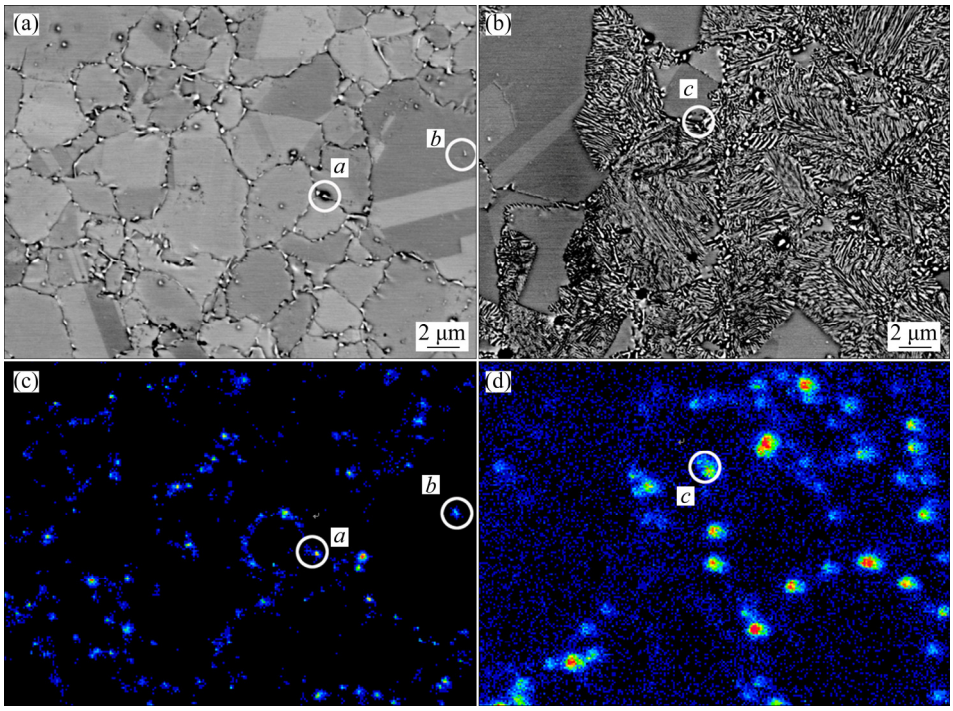

Fig. 2 BSE images and corresponding Nb element maps of Cu−15Ni−8Sn−0.3Nb alloy: (a, c) Solution-treated at 850 °C for 1 h; (b, d) Aged at 400 °C for 3 h

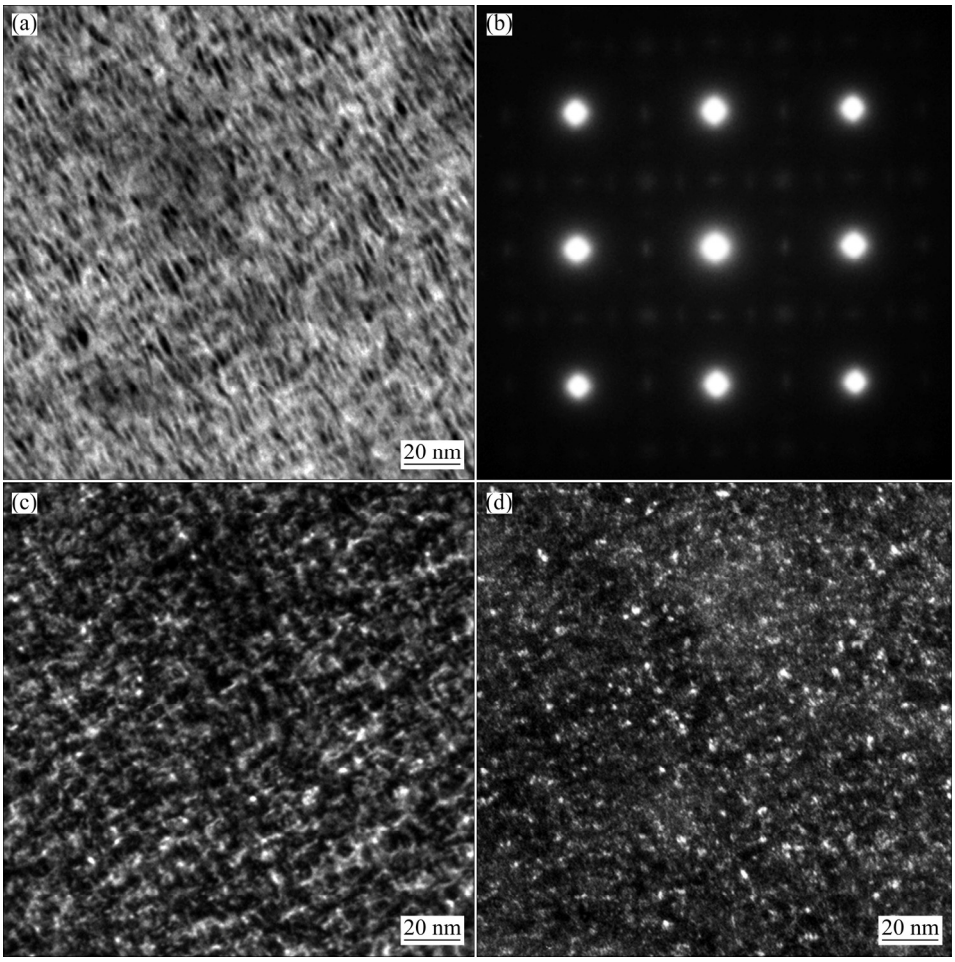

Fig. 3 TEM images of Cu−15Ni−8Sn−0.3Nb alloy specimen aged at 400 °C for 0.25 h: (a) Morphology of matrix; (b) SADP along [001] direction; (c, d) Bright-field and central-dark field images, respectively

Bright-field and central dark-field images of this specimen were taken by using either matrix reflections or the (011) supperlattice reflections, as shown in Figs. 3(c) and (d), respectively. For the Cu−Ni−Sn alloys, DO_{22}-ordered phases adopt needle-like morphology to reduce elastic strain energy and grow along direction *c*, which is parallel to the three [001] directions of the FCC matrix [14,23]. Therefore, there are three variants for the DO_{22}-ordered phases. For $L1_2$ ordering, there is only one variant because the $L1_2$-ordered phases are still FCC structure and coherent with the Cu matrix[24]. The bright dots in Fig. 3(d) are ordered phases. However, it is difficult to identify the ordering type of each bright dot because clear dark-field images are captured only when using the {011}-type reflections which belong to both DO_{22} and $L1_2$ ordering.

A bright-field image and the corresponding SADP of a Cu−15Ni−8Sn−0.3Nb alloy specimen aged at 400 °C for 1.25 h are shown in Fig. 4. A small amount of discontinuous precipitates were observed in Fig. 4(a). The corresponding SADP along [001] direction is shown in Fig. 4(b). Compared with Fig. 3(b), the superlattice reflections of $L1_2$ ordering in Fig. 4(b) became stronger and the superlattice reflections of DO_{22} ordering became weaker, which indicated that the transition from DO_{22} to $L1_2$ ordering occurred [17].

Figure 5 shows TEM images and the corresponding SADP of a Cu−15Ni−8Sn−0.3Nb alloy specimen aged at 400 °C for 6 h. Large amounts of discontinuous precipitates were observed in Fig. 5(a). Many intragranular and intergranular *γ*-precipitates were embedded in the *α*-matrix, as marked by arrows in Fig. 5(b). The corresponding SADP along [001] direction is shown in Fig. 5(c). It is obvious that the {001}- and {011}-type superlattice reflections became dominant and the {0 1/2 1}-type superlattice reflections nearly disappeared, which meant that the transition from DO_{22} to $L1_2$ ordering was completed.

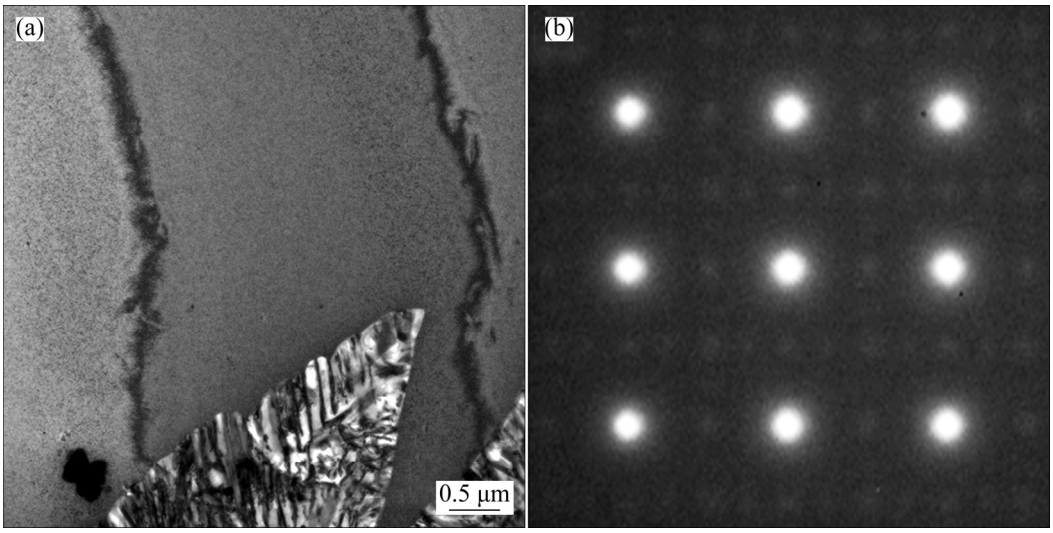

Fig. 4 TEM images of Cu−15Ni−8Sn−0.3Nb alloy specimen aged at 400 °C for 1.25 h: (a) Bright-field image of matrix; (b) SADP along [001] direction

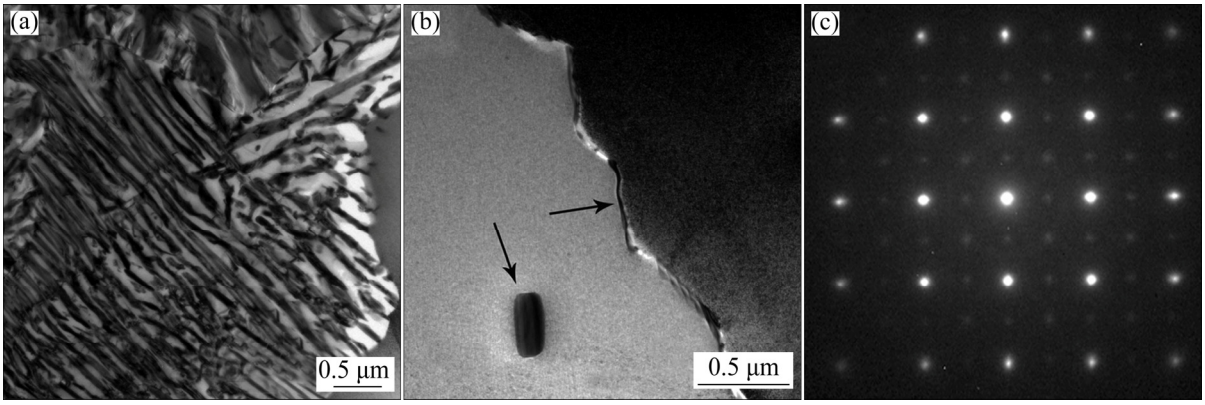

Fig. 5 TEM images of Cu−15Ni−8Sn−0.3Nb alloy specimen aged at 400 °C for 6 h: (a) Bright-field image showing large amount of discontinuous precipitates; (b) Intergranular and intragranular *γ*-precipitates in residual matrix, as marked by arrows; (c) Corresponding SADP along [001] direction

ZHAO and NOTIS [17] established a TTT diagram of Cu−15Ni−8Sn alloy which indicated that intragranular and intergranular γ-phases could occur only during aging treatment at above 600 °C. However, in the present study, intragranular and intergranular γ-phases were easily observed in both Cu−15Ni−8Sn−0.3Nb and Cu−15Ni−8Sn alloy specimens aged at 400 °C. TEM characterization was conducted for the solution-treated Cu−15Ni−8Sn−0.3Nb alloy specimen, as shown in Fig. 6. As shown in Fig. 6(a), intragranular (Circle 1) and intergranular γ-precipitates (Circle 2) were observed in the solution-treated specimen. Therefore, it was confirmed that intragranular and intergranular γ-phases precipitated during water quenching after solution treatment. The explanation is possible that the cooling rate was not high enough during water-quenching for bulk alloys, which led to the precipitation. The corresponding SADPs of the precipitates are shown in Figs. 6(b) and (c), respectively. Figure 6(b) shows that there are only two diffraction spots of the intragranular γ-precipitate in Circle 1 (marked by the arrows). Figure 6(c) shows that no diffraction spots of the intergranular γ-precipitate exist in Circle 2. The two SADPs indicate that there is no orientation relationship between the FCC matrix and the intragranular and intergranular γ-precipitates.

3.4 STEM images

High angle annular dark field (HAADF) images and the corresponding element maps of different precipitates of aged Cu−15Ni−8Sn−0.3Nb alloy specimens are shown in Fig. 7. The solubility of Nb in Cu matrix is limited [25], and there are several kinds of intermetallic compounds (IMCs) between Ni and Nb, such as Ni_3Nb and Ni_6Nb_7 [26]. Therefore, it is possible to find Nb-rich phases or IMCs between Nb and Ni in the Cu−15Ni−8Sn−0.3Nb alloy. Figures 7(a) and (b) show a HAADF image of a intergranular γ-precipitates and the corresponding element maps, respectively. The intergranular precipitate is rich in Ni, Sn, Nb and poor in Cu. A HAADF image of an area containing discontinuous precipitates and several intragranular γ-precipitates is shown in Fig. 7(c) and the corresponding element maps are shown in Fig. 7(d). The element maps showed that an evident enrichment of Nb was found in the intragranular γ-precipitates and no enrichment of Nb was found in the discontinuous precipitates. The results of element maps indicated that Nb was localized within the grains and along the grain boundaries. It should be noted that the precipitates in Figs. 7(a) and (c) are brighter than the surrounding matrix, which indicates the existence of heavy elements in those precipitates [10,27]. The heavy element in Cu−Ni−Sn alloys is Sn. Therefore, the results accord well with the general understanding that γ-precipitates in Cu−Ni−Sn alloys are Sn-rich phases.

Table 2 presents the EDS results of several phases in aged Cu−15Ni−8Sn−0.3Nb alloy specimens. It shows an evident enrichment of Nb in the intragranular γ-precipitates (containing 29.26% Nb, mass fraction) and a slight enrichment of Nb in the intergranular γ-precipitates (containing 2.33% Nb, mass fraction). However, Nb enrichment is not found in the matrix and the discontinuous precipitates, which accords with the element maps shown in Figs. 7(b) and (d).

3.5 Mechanical properties

The tensile properties of Cu−15Ni−8Sn−xNb alloys are shown in Fig. 8. Both strength and ductility were improved by the addition of Nb. Firstly, stable plateaus was obtained in the plots of both the ultimate tensile strength (UTS) and yield strength (YS) of Cu−15Ni−8Sn−0.3Nb alloy specimens aged for less than 1.25 h. The plateau values of UTS and YS are above 1030 and 880 MPa, respectively. The plateau values are higher than the peak UTS (1017 MPa) and YS (799 MPa) of the Cu−15Ni−8Sn alloy. The higher strength during aging for less than 1.25 h is attributed to the addition of Nb into Cu−15Ni−8Sn alloy, which leads to smaller

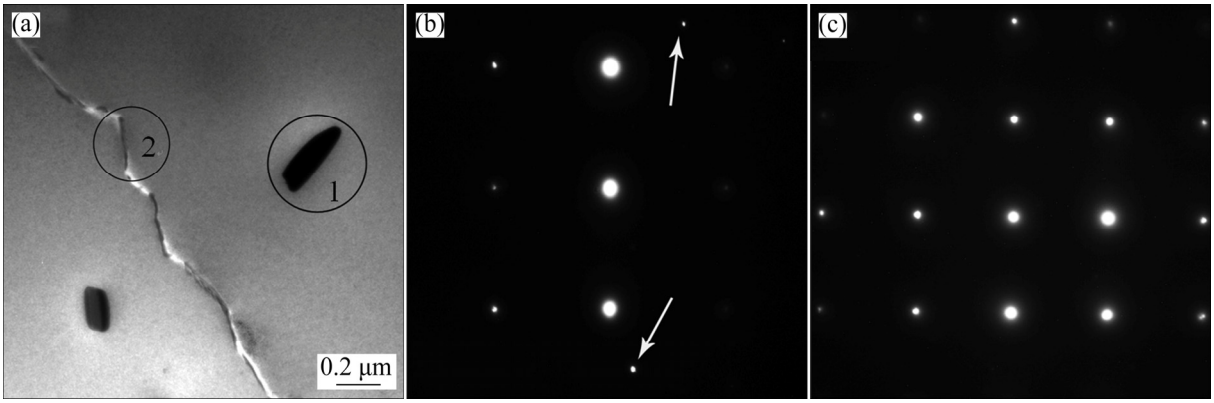

Fig. 6 TEM images of solution-treated Cu−15Ni−8Sn−0.3Nb alloy specimen: (a) Bright-field image of matrix; (b) Corresponding SADP of intragranular precipitate in Circle 1; (c) Corresponding SADP of intergranular precipitate in Circle 2

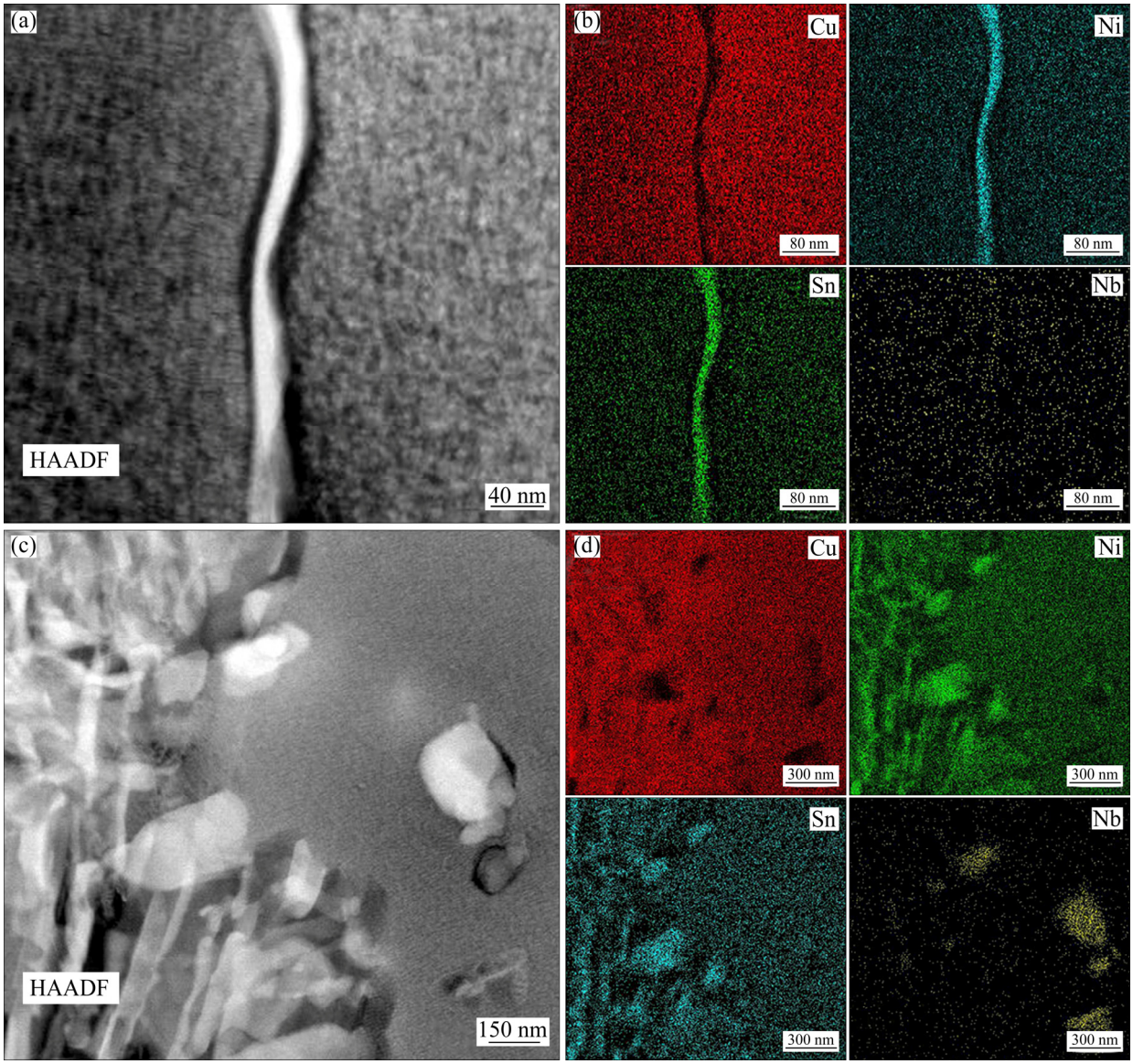

Fig. 7 HAADF images (a, c) and corresponding element maps (b, d): (a, b) Intergranular γ-precipitate; (c, d) Area containing both intragranular γ-precipitates and discontinuous precipitates

Table 2 EDS results of Cu−15Ni−8Sn−0.3Nb alloy specimens after aging treatment (mass fraction, %)

Phase	Cu	Ni	Sn	Nb
Matrix	75.19	15.22	9.46	0.13
Intragranular γ	54.60	11.56	4.58	29.26
Intergranular γ	61.25	26.16	10.26	2.33
DP	27.24	48.28	24.30	0.18

grain size and less amount of discontinuous precipitates. The tensile strength dropped sharply from 1030 to 885 MPa after aging for 1.25−1.5 h for Cu−15Ni−8Sn−0.3Nb alloy, which could be ascribed to the growth of discontinuous precipitates [5,10].

Comparing Figs. 8(b) with (d), it is obvious that the addition of Nb also improved ductility. As proved in Ti−Ni binary alloys, the introduction of soft phases is an effective way to improve the mechanical properties of brittle materials [19]. Therefore, the higher ductility in the Cu−15Ni−8Sn−0.3Nb alloy is probably caused by the formation of Nb-rich soft phases. It is noteworthy that the ductility increased in both Cu−15Ni−8Sn−0.3Nb and Cu−15Ni−8Sn alloys in over-aged conditions. In the present research, the dominant phase in over-aged conditions was discontinuous precipitates, as shown in Fig. 5(a). Therefore, the increase in ductility should be related to the growth of discontinuous precipitates. When the coherent internal stress field produced by spinodal decomposition and ordering was decomposed by discontinuous precipitates, the ductility of Cu−15Ni−8Sn−xNb alloys increased with further aging.

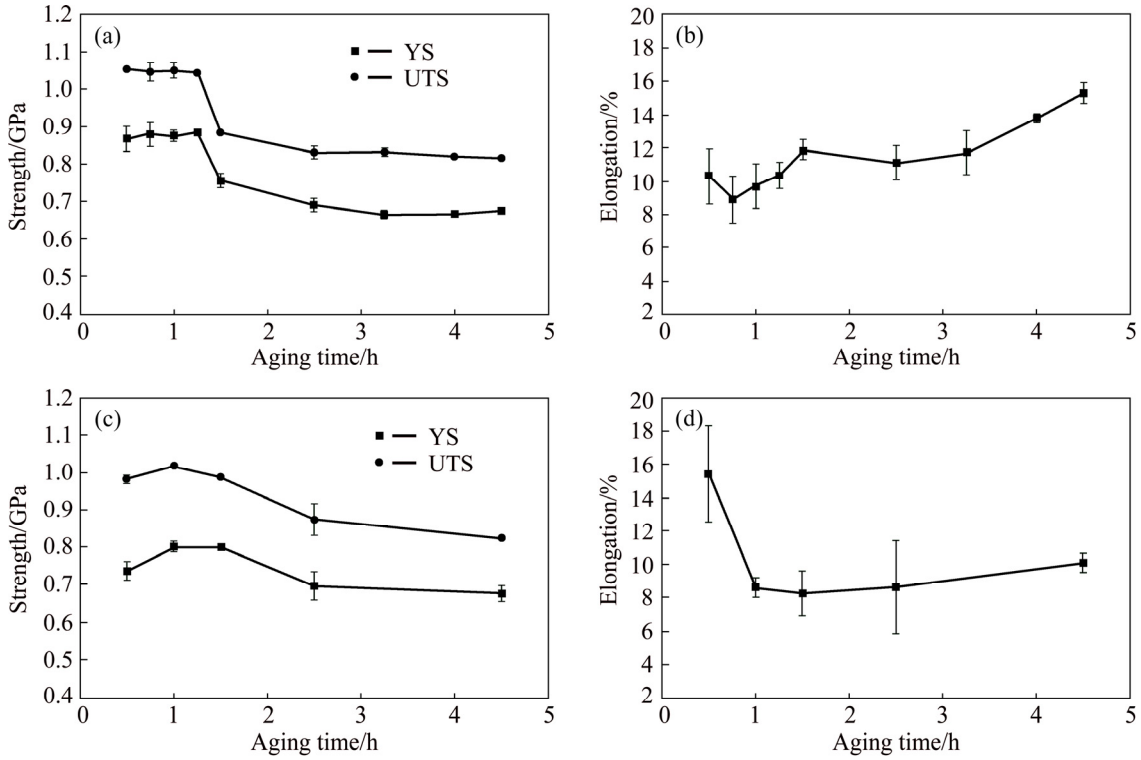

Fig. 8 Mechanical properties of Cu−15Ni−8Sn−0.3Nb (a, b) and Cu−15Ni−8Sn (c, d) alloy specimens after aging at 400 °C for 0.5−4.5 h

4 Conclusions

1) The addition of Nb resulted in the formation of intragranular and intergranular Nb-rich γ-precipitates after solution treatment, which inhibited the grain coarsening and postponed the growth of discontinuous precipitates during aging treatment.

2) Compared with the Cu−15Ni−8Sn alloy, the Cu−15Ni−8Sn−0.3Nb alloy exhibited both higher strength (ultimate tensile strength >1030 MPa) and higher tensile ductility (elongation>9.1%) after aging for 0.5−1.25 h. The improvement in strength is attributed to the smaller grain size and less discontinuous precipitates, and the improvement in ductility resulted from the introduction of ductile Nb-rich phases.

References

[1] SINGH J B, CAI W, BELLON P. Dry sliding of Cu−15wt%Ni−8wt% Sn bronze: Wear behaviour and microstructures [J]. Wear, 2007, 263(1): 830−841.

[2] HERMANN P H, MORRIS D G. Relationship between microstructure and mechanical properties of a spinodally decomposing Cu−15Ni−8Sn alloy prepared by spray deposition [J]. Metallurgical and Materials Transactions A, 1994, 25(7): 1403−1412.

[3] FANG S F, WANG M P, WANG Y H, QI W H, LI Z. Evolutionary artificial neural network approach for predicting properties of Cu−15Ni−8Sn−0.4Si alloy [J]. Transactions of Nonferrous Metals Society of China, 2008, 18(5): 1223−1228.

[4] GAHN J W. Hardening by spinodal decomposition [J]. Acta Metallurgica, 1963, 11(12): 1275−1282.

[5] CARPENTER R W. Deformation and fracture of gold−platinum polycrystals strengthened by spinodal decomposition [J]. Acta Metallurgica, 1967, 15(8): 1297−1308.

[6] SCHWARTZ L H, PLEWES J T. Spinodal decomposition in Cu−9wt%Ni−6wt%Sn—II. A critical examination of mechanical strength of spinodal alloys [J]. Acta Metallurgica, 1974, 22(7): 911−921.

[7] SATO A, TAMURA K, ITO M, KATO M, MORI T. In situ observation of moving dislocations in a Cu−10Ni−6Sn spinodal alloy [J]. Acta Metallurgica et Materialia, 1993, 41(4): 1047−1055.

[8] SAHU P, PRADHAN S K, DE M. X-ray diffraction studies of the decomposition and microstructural characterization of cold-worked powders of Cu−15Ni−Sn alloys by Rietveld analysis [J]. Journal of Alloys and Compounds, 2004, 377(1): 103−116.

[9] RHU J C, KIM S S, JUNG Y C, HAN S Z, KIM C J. Tensile strength of thermomechanically processed Cu−9Ni−6Sn alloys [J]. Metallurgical and Materials Transactions A, 1999, 30(10): 2649−2657.

[10] WESTRAADT J E, OLIVIER E J, NEETHLING J H, HEDSTROM P, ODQVIST J, XU X, STEUWER A. A high-resolution analytical scanning transmission electron microscopy study of the early stages of spinodal decomposition in binary Fe−Cr [J]. Materials Characterization, 2015, 109: 216−221.

[11] SCHWARTZ L H, MAHAJAN S, PLEWES J T. Spinodal decomposition in a Cu−9wt%Ni−6wt%Sn alloy [J]. Acta Metallurgica, 1974, 22(5): 601−609.

[12] CARIS J, VARADARAJAN R, STEPHENS J J, LEWANDOWSKI J J. Microstructural effects on tension and fatigue behavior of Cu−15Ni−8Sn sheet [J]. Materials Science and Engineering A, 2008, 491(1): 137−146.

[13] DITCHEK B, SCHWARTZ L H. Diffraction study of spinodal decomposition in Cu−10wt%Ni−6wt%Sn [J]. Acta Metallurgica, 1980, 28(6): 807−822.
[14] LEFEVRE B G, D′ANNESSA A T, KALISH D. Age hardening in Cu−15Ni−8Sn alloy [J]. Metallurgical Transactions A, 1978, 9(4): 577−586.
[15] SPOONER S, LEFEVRE B G. The effect of prior deformation on spinodal age hardening in Cu−15Ni−8Sn alloy [J]. Metallurgical Transactions A, 1980, 11(7): 1085−1093.
[16] KROTACHVIL P, MENCL J, PESICKA J, KOMNIK S N. The structure and low temperature strength of the age hardened Cu−Ni−Sn alloys [J]. Acta Metallurgica, 1984, 32(9): 1493−1497.
[17] ZHAO J C, NOTIS M R. Spinodal decomposition, ordering transformation, and discontinuous precipitation in a Cu−15Ni−8Sn alloy [J]. Acta Materialia, 1998, 46(12): 4203−4218.
[18] SCOREY C R, CHIN S, WHITE M J, LIVAK R J. Spinodal Cu−Ni−Sn alloys for electronic applications [J]. Journal of Materials, 1984, 36(11): 52−54.
[19] KIM H Y, JINGUU T, NAM T H, MIYAZAKI S. Cold workability and shape memory properties of novel Ti−Ni−Hf−Nb high-temperature shape memory alloys [J]. Scripta Materialia, 2011, 65(9): 846−849.
[20] HSIEH S F, WU S K, LIN H C, YANG C H. Transformation sequence and second phases in ternary Ti−Ni−W shape memory alloys with less than 2at.%W [J]. Journal of Alloys and Compounds, 2005, 387(1): 121−127.
[21] NING Y, ZHOU C, LIANG H, FU M W. Abnormal flow behavior and necklace microstructure of powder metallurgy superalloys with previous particle boundaries (PPBs) [J]. Materials Science and Engineering A, 2016, 652: 84−91.
[22] ALILI B, BRADAI D, ZIEBA P. On the discontinuous precipitation reaction and solute redistribution in a Cu−15%Ni−8%Sn alloy [J]. Materials Characterization, 2008, 59(10): 1526−1530.
[23] LI R, DUAN Y. Electronic structures and thermodynamic properties of $HfAl_3$ in $L1_2$, DO_{22} and DO_{23} structures [J]. Transactions of Nonferrous Metals Society of China, 2016, 26(9): 2404−2412.
[24] ZHANG M Y, LI Z G, ZHANG J L, ZHANG H Z, CHEN Z, ZHANG J Z. Site occupation evolution of alloying elements in Ni_3V phase during phase transformation in $Ni_{75}Al_{4.2}V_{20.8}$ [J]. Transactions of Nonferrous Metals Society of China, 2015, 25(5): 1599−1604.
[25] VERHOEVEN J D, DOWNING H L, CHUMBLEY L S, GIBSON E D. The resistivity and microstructure of heavily drawn Cu−Nb alloys [J]. Journal of Applied Physics, 1989, 65(3): 1293−1301.
[26] YANG G J, HAO S M. Study on the phase equilibria of the Ti−Ni−Nb ternary system at 900 °C [J]. Journal of Alloys and Compounds, 2000, 297(1): 226−230.
[27] MIDGLEY P A, WEYLAND M. 3D electron microscopy in the physical sciences: The development of Z-contrast and EFTEM tomography [J]. Ultramicroscopy, 2003, 96(3): 413−431.

粉末冶金法结合热挤压制备 Cu−15Ni−8Sn−0.3Nb 合金的时效硬化行为与显微组织

欧阳亦[1]，甘雪萍[1]，张世忠[1]，李 周[2]，周科朝[1]，姜业欣[2,3]，张县委[2,3]

1. 中南大学 粉末冶金国家重点实验室，长沙 410083；
2. 中南大学 材料科学与工程学院，长沙 410083；
3. 中色奥博特铜铝业有限公司，聊城 252600

摘 要：采用粉末冶金法结合热挤压制备 Cu−15Ni−8Sn−0.3Nb 合金棒材。利用电子探针获得的元素分布图显示，在合金基体中生成了分布在晶界与晶内的富 Nb 析出相。透射电镜分析表明，富 Nb 析出相与合金基体之间无明确位向关系。合金在 400 °C 时效早期发生调幅分解和有序化，使其强度迅速升高。Cu−15Ni−8Sn−0.3Nb 合金比 Cu−15Ni−8Sn 合金具有更高的强度(抗拉强度>1030 MPa)和更好的延性(伸长率>9.1%)，这是由于添加 Nb 元素后生成的富 Nb 析出相能细化合金组织，抑制时效过程中的胞状析出。

关键词：Cu−15Ni−8Sn−0.3Nb 合金；粉末冶金法； 热挤压；时效处理；调幅分解；显微组织；力学性能

(Edited by Wei-ping CHEN)